In vitro solubilization of fat-soluble vitamins in structurally defined mixed intestinal assemblies

Asma El Aoud, Emmanuelle Reboul, Aurélien Dupont, Cristelle Mériadec, Franck Artzner, Sébastien Marze

HAL Id: hal-03122063
https://hal.inrae.fr/hal-03122063

Submitted on 28 Jan 2021

1 **In vitro solubilization of fat-soluble vitamins in structurally defined mixed intestinal**

2 **assemblies**

3

4 Asma El Aoud,[1,2] Emmanuelle Reboul,[2] Aurélien Dupont,[3] Cristelle Mériadec,[4] Franck Artzner,[4] and

5 Sébastien Marze[1*]

6

7 1 INRAE, BIA, F-44316, Nantes, France

8 2 AMU, INRAE, INSERM, C2VN, Marseille, France

9 3 CNRS, Biosit, UMS 3480, Université de Rennes 1, US_S 018, F-35000, Rennes, France

10 4 CNRS, Institut de Physique de Rennes, UMR 6251, Université de Rennes 1, F-35000, Rennes, France

11 * Corresponding author: sebastien.marze@inrae.fr

12

13 **Abstract**

14 The structures of fed state intestinal assemblies containing bile components, dietary fat, and fat-

15 soluble vitamins are not well known, although they are involved in lipid transport. In this study, several

16 methods were used to investigate structural transitions upon various dietary lipids or various fat-

17 soluble vitamins incorporation in bile intestinal assemblies. In particular, DLS and turbidimetry were

18 used to study transition points as a function of component concentration, and cryo-TEM and SAXS

19 were used to resolve assembly structures at microscopic and supramolecular scales, respectively.

20 Results showed that increasing the concentration of dietary lipids in bile assembly induced a transition

21 from core-shell micelles to unilamellar vesicles (except with caprylate lipids, always yielding micelles).

22 In these specific assemblies, increasing the concentration of a fat-soluble vitamin either induced a

23 systematic structural transition, defining a solubilization capacity (α-tocopherol or phylloquinone), or

24 induced a structural transition only in micelles (retinol), or did not induce any structural transition up

25 to very high concentrations (cholecalciferol). Using SAXS data, ideal molecular organizations are

26 proposed for assemblies in the absence or presence of α-tocopherol.

27

28 **Keywords**: micelle, vesicle, lipid, bile, fat-soluble vitamin, solubilization, SAXS, cryo-TEM

29

30 **1. Introduction**

31 Upon the ingestion of food or medication, many physicochemical processes occur in the

32 gastrointestinal tract to make nutrients or drugs bioaccessible (absorbable by the intestinal cells).

33 These processes typically include mechanical breakdown, dissolution, enzymatic hydrolysis, molecular

34 solubilization, and binding to specific carriers.

35 For lipids and lipophilic compounds, molecular solubilization in luminal water is actually insignificant,

36 as their aqueous solubility is very low. Instead, transport to their absorption site takes place in

37 supramolecular structures, usually called micelles, aggregates, or assemblies, composed of molecules

38 secreted in the bile.

39 Thus, to be transported, lipids and lipophilic compounds have to be solubilized (i.e. incorporated) in

40 bile assemblies. This critical step for absorption is commonly studied for poorly water-soluble drugs,

41 but rarely for lipophilic nutrients. Solubilization ratio (defined as the molar or mass ratio of lipophilic

42 compound to micellar bile salt) values are thus mainly available for drugs, although some data exist for

43 fat-soluble vitamins (Wiedmann and Kamel, 2002).

44 In any case, assembly structure is an important aspect that was only reported in a few articles. It is

45 indeed known from the seminal works of Small and/or Carey that physiological surfactants (such as

46 bile salts and phospholipids) form various types of assembly, spherical micelles described for many

47 synthetic surfactants only occurring in specific conditions (Carey and Small, 1970; Muller, 1981; Phan

48 et al., 2015). For gallbladder bile, bilayer disk shapes (Small et al., 1969; Mazer et al., 1980; Muller,

49 1981; Madenci et al., 2011) and long cylinder shapes (Ulmius et al., 1982; Nichols and Ozarowski, 1990;

50 Hjelm et al., 1992; Cohen et al., 1998) were mainly reported for bile salt-phospholipid systems, with a

51 transition from small disks to large vesicles when cholesterol was added (Mazer and Carey, 1983). This

52 transition was later found in the absence of cholesterol but upon dilution (Schurtenberger et al., 1985).

53   Intermediate transitions were also found upon temporal rearrangement (Egelhaaf and

54   Schurtenberger, 1999), from cylinders to disks to vesicles, the longest lived assemblies being disks and

55   vesicles (Leng et al., 2003).

56   For intestinal bile, containing diluted bile and fat digestion products (fatty acid FA and monoglyceride

57   MG), disks and vesicles were found to coexist in the duodenal fluid of fed healthy humans (Hernell et

58   al., 1990), which could be reproduced in vitro (Staggers et al., 1990). The coexistence of micelles and

59   vesicles was again observed recently in the duodenal fluid of both fasted and fed healthy humans

60   (Elvang et al., 2016; 2019), and reproduced in vitro, obtaining disk-like micelles and polydisperse

61   vesicles (Elvang et al., 2016; 2018). However, an accurate characterization of standard simulated

62   intestinal fluids using small-angle X-ray scattering (SAXS) contradicted this coexistence, multilamellar

63   vesicles being only present in the fasted state, and core-shell ellipsoidal micelles being the only

64   assembly in the fed state (Clulow et al., 2017). Moreover, ellipsoidal micelles were also identified in

65   the fed state using small-angle neutron scattering (Rezhdo et al., 2017).

66   In the context of poorly water-soluble drug solubilization, the seminal works of Kossena et al. (2003;

67   2004) revealed transitions between mixed intestinal assemblies upon FA+MG addition. In their first

68   article, they reported the coexistence of micelles and vesicles in both the fasted state (low bile

69   concentration) and the fed state (high bile concentration), drug solubilization being higher in the

70   presence of digestion products, and in the fed state (Kossena et al., 2003). In their second article, in

71   the fasted state, they confirmed the coexistence of micelles and vesicles, the latter being unilamellar

72   or multilamellar at low or high FA+MG concentration, respectively. At even higher FA+MG

73   concentration, lamellar liquid crystal or cubic liquid crystal were found depending on the type of FA

74   and MG (C8:0, caprylate; C12:0, laurate; C18:1; oleate). Drug solubilization was higher at higher FA+MG

75   concentration, and in liquid crystal phases (Kossena et al., 2004). Later, the same research group

76   reported a transition from pure micelles to coexisting micelles and vesicles with increasing FA+MG

77   concentration in the fasted state, leading to drug solubilization increase (Birru et al., 2017). Finally,

78   Ilardia-Arana et al. (2006) and Kleberg et al. (2010) also reported a transition from pure micelles to

79   coexisting micelles and vesicles with increasing FA+MG concentration in both fasted and fed states,

80   leading to drug solubilization increase.

81   Although these works clearly identified the transitions and the various assemblies obtained in the

82   presence of FA+MG, their structures upon drug solubilization were only characterized once (Nielsen et

83   al., 2001). Moreover, only drug solubilization was investigated using this approach, and no systematic

84   study was reported for the solubilization of fat-soluble vitamins.

85   To fill these gaps, we conducted a systematic solubilization study of fat-soluble vitamins using a

86   relevant composition of intestinal bile (including lysophosholipids) in the fed state. First, the effect of

87   increasing FA+MG concentration in intestinal bile assemblies was determined as a function of FA and

88   MG type (C8:0, C18:1, C22:6, docosahexaenoate). Both the concentration and the type of FA and MG

89   were indeed anticipated to influence assembly structures and transitions. Several techniques

90   (turbidimetry, cryo-TEM, DLS, SAXS) were used to cover macroscopic to molecular scales, enabling the

91   characterization of two distinct assemblies. Then, the solubilization capacity, expected to depend on

92   the structure and composition of these assemblies, was determined by addition of increasing amounts

93   of fat-soluble vitamins, checking assembly structures and transitions using the same techniques.

94

95   **2. Materials**

96   Sodium taurocholate (86339), the lysophosphatidylcholines (855675P, 845875P), cholesterol (C3045),

97   cholecalciferol (C9756), retinol (95144), phylloquinone (95271), and α-tocopherol (T3251) were

98   purchased from Sigma-Aldrich, France. Phosphate-buffered saline (PBS; 155 mM NaCl, 2.7 mM

99   Na_2HPO_4-$7H_2O$, 1.5 mM KH_2PO_4) pH 7.2 (20012019) was purchased from Thermo Fisher Scientific,

100   France. Caprylic acid (N-8-A), palmitic acid (N-16-A), oleic acid (U-46-A), docosahexaenoic acid (U-84-

101   A), monocaprylin (M-114), monoolein (M-239), and monodocosahexaenoin (M-314) were purchased

102   from Nu-Chek Prep, USA.

103

104   **3. Methods**

105   **3.1. Intestinal bile compositions**

106   Simple intestinal bile (SIB) composition was designed to mimic that in the duodenal lumen of the

107   mouse. Bile salt concentration was found to be around 20 mM in mouse upper intestine (Tannock et

108   al., 1994). Based on mouse biliary output ratios between bile salt, phospholipid and cholesterol

109   (Werner et al., 2002; Kok et al., 2003), we deduced phospholipid and cholesterol concentrations in

110   mouse upper intestine of 3 mM and 0.25 mM, respectively. To simplify the system, we used the most

111   abundant bile salt in the mouse, taurocholate (Baghdasaryan et al., 2016; Pathak et al., 2018), and also

112   the most abundant phospholipids, phosphatidylcholines containing 16:0 or 18:1 fatty acids (Agellon et

113   al., 1999). Each phospholipid was included in the system as one lysophosphatidylcholine plus one free

114   fatty acid. The resulting composition is reported in table 1.

115

Concentration	TC	16:0 LPC	18:1 LPC	PA	OA	CH
mM	19	1.55	1.45	1.55	1.45	0.25
mg mL^{-1}	10	0.75	0.75	0.40	0.40	0.10

116

117   Table 1: Composition of the simple intestinal bile SIB (TC: taurocholate, LPC: lysophosphatidylcholine, PA:

118   palmitic acid, OA: oleic acid, CH: cholesterol).

119

120   The range of FA+MG addition to the SIB to make the mixed intestinal assemblies was determined by

121   estimating a mass ratio of fat intake to bile salt output in vivo in the rat (no data available for the

122   mouse). This ratio was typically comprised between 3.0 and 7.0 for ad libitum diets (Boquillon and

123   Clement, 1979; Sugano et al., 1983). However, for restricted diets, this ratio could be as low as 0.5, as

124   found in the human (Grundy and Metzger, 1972) and in the pig (Juste et al., 1983). We thus selected a

125   range between 0.5 and 4.0 for the FA+MG/TC mass ratio, keeping a FA:MG molar ratio of 2:1, as

126   obtained upon triglyceride hydrolysis by gastrointestinal lipases. The resulting FA and MG

127   concentrations used are reported in table 2.

128

Concentration	CA	MC	OA	MO	DHA	MDH
mM	19.8-158	9.9-79	10.8-86	5.5-44	9.6-77	4.6-37
mg mL^{-1}	2.85-22.8	2.15-17.2	3.05-24.4	1.95-15.6	3.15-25.2	1.85-14.8

129

130 Table 2: Concentration ranges of FA and MG added to the simple intestinal bile SIB to make mixed intestinal

131 assemblies (CA: caprylic acid, MC: monocaprylin, OA: oleic acid, MO: monoolein, DHA: docosahexaenoic acid,

132 MDH: monodocosahexaenoin). The total mass concentration range of FA+MG is invariable, between 5.0 and 40.0

133 mg mL^{-1}. Note that molar concentrations depend on FA and MG type, resulting in FA+MG/TC molar ratios

134 between 0.75 and 12.5, especially different for the CA+MC systems.

135

136 Finally, the ranges of vitamin addition to the mixed intestinal assemblies, reported in table 3, were

137 estimated from literature values of i) rodent vitamin intake (Reeves et al., 1993), as the absorption of

138 vitamins from these assemblies will be later tested in the mouse, ii) human upper vitamin intake to

139 select the maximal values, and iii) mass solubilization ratios (SR, defined here as the ratio of the

140 lipophilic compound mass to the taurocholate mass), which will be discussed later.

141

142

143

144

145

146

	Cholecalciferol	Retinol	Phylloquinone	α-tocopherol
M (g mol^{-1})	384.64	286.45	450.70	430.71
C (mM)	$0.78.10^{-3}$-7.8	0.0175-17.5	0.222-22.2	1.16-73.1

C (mg mL^{-1})	0.3.10^{-3}-3	5.10^{-3}-5	0.1-10	0.5-31.5
SR (mg mg^{-1} TC)	0.03.10^{-3}-0.3	0.5.10^{-3}-0.5	0.01-1	0.05-3.15

147

148   Table 3: Molar mass (M), concentration (C), and SR ranges of vitamins added to the mixed intestinal assemblies.

149

150   **3.2. Sample preparation**

151   Stock solutions in chloroform/methanol (2:1 v:v) were prepared by weighing i) the components of

152   simple intestinal bile (except taurocholate), ii) the fatty acid and monoglyceride, and iii) the vitamin.

153   These stock solutions were prepared in a dark room, stored in the dark at room temperature, and used

154   within 5 days. To prepare the samples (usually 11 samples simultaneously), appropriate volumes of

155   each solution were transferred to small volume amber vials to bring the correct mass for each

156   component, with a maximal total volume of 2 mL. The chloroform/methanol solvent was then totally

157   evaporated under nitrogen until a lipid film was obtained. Finally, 2 mL of 10 mg mL^{-1} taurocholate

158   solution in PBS was added, yielding samples with concentrations indicated in tables 1-2-3. These

159   samples were kept at rest for 1 hour to ensure total hydration of the lipid film.

160   The samples were transferred to round bottom 1 cm plastic tubes for individual sonication using a

161   Misonix Sonicator 4000 equipped with a microtip probe 419 (Qsonica, Connecticut, USA). During the

162   sonication, the sample was kept on ice to prevent temperature increase. Each sample was sonicated

163   for 5 min at 15 W, bringing a total energy of 4.5 kJ, with 1 min pause each 1 min sonication, again to

164   prevent temperature increase. Then, the pH of each sample, measured with a microelectrode (HI1083,

165   Hanna Instruments, France), was brought to 7.0 ± 0.1 using 10 to 30 µL of 2M NaOH. Finally, each

166   sample was filtered using a 0.22 µm porosity RC membrane (Minisart 17821 K, Sartorius). Whenever

167   vitamin was present in the sample, a preliminary filtration using a 0.45 µm porosity RC membrane

168   (Phenex AF0-2103-12, Phenomenex) was performed to prevent plugging of the 0.22 µm filter. All

169   samples were stored in the dark at room temperature, and characterized within 48 hours after

170 preparation (24 hours in the presence of vitamin). Each sample was prepared at least twice, on

171 different days.

3.3. Sample characterization

173 Results are expressed as average ± standard deviation, except where noted. In most figures,

174 independent samples are shown, the error bar of several measurements on a specific sample being

175 within the symbol size.

3.3.1. Dynamic light scattering

177 Back-scattering size distribution measurement was performed at 20 °C using a Zetasizer Nano ZS

178 dynamic light scattering (DLS) apparatus (Malvern Instruments Ltd, Worcestershire, UK) equipped with

179 a 4 mW He-Ne laser at λ = 633 nm. The exact angle between the laser beam and the detector

180 (avalanche photodiode) is 173. The refractive index value for the PBS was set to 1.33. For the lipids,

181 the refractive index of the most abundant lipid was used for each system, that is 1.43, 1.46, 1.52, or

182 1.56 for CA, OA, DHA, or TC, respectively. It was checked that the results were the same when the

183 refractive index of the lipid mixtures was estimated according to the real composition of each system.

184 The absorption was always set to 0.001. Undiluted samples of 1 mL were placed in disposable 12 mm

185 square polystyrene cuvettes with 1 mm thick walls (Brand, Wertheim, Germany). A 30 s acquisition

186 time was used to obtain a stable autocorrelation function. For each sample, the result is given as the

187 average of the number-based mean diameter over 10 to 20 measurement repetitions.

3.3.2. Turbidimetry

189 The turbidity of 1 mL undiluted samples was measured at 20 °C in the same disposable cuvettes,

190 characterized as the absorbance at λ = 600 nm using a transmission UV-vis spectrophotometer (UV-

191 1800, Shimadzu, France).

3.3.3. Small-angle X-ray scattering

193 A home-made laboratory SAXS setup was used (Bizien et al., 2015) to analyze the structural

194 organization of the samples. Scattering results were collected with a Pilatus 300 K (Dectris,

195 Switzerland), mounted on a microsource X-ray generator GeniX 3D (Xenocs, France) operating at 30 W.

196   The monochromatic CuKα radiation of $\lambda = 1.541$ Å is selected by an asymmetric multilayer mirror

197   (Xenocs, France), and the beam is defined by two sets of slits. The results were recorded in a reciprocal

198   space $q = (4\pi.\sin\theta)/\lambda$ in a range of repetitive distances from 0.013 to 1.72 Å^{-1}. The channel to scattering

199   vector (q) calibration of the detector was carried out with silver behenate.

200   Samples of 10 µL were placed in thin quartz capillaries of 1.5 mm diameter (GLAS W. Muller, Berlin,

201   Germany) for the measurements. Up to 19 samples were measured successively at 20 °C, with 1 hour

202   of acquisition for each sample. The pure solvent (PBS at pH 7.0) was always one of the samples,

203   enabling the subtraction of the solvent background intensity in the analysis of the other samples,

204   proportionally to the amount of solvent they contain.

205   The intensity profiles were modelled using SasView v4.1.2. Based on the literature results, the core-

206   shell cylinder (able to fit both flat disk and long cylinder), the core-shell ellipsoid (able to fit both oblate

207   and prolate ellipsoid), and the core-multi-shell sphere (a core-shell sphere with a given number of

208   shells) models were tested (see SasView website). Their parameters were the same, being the

209   background intensity, the intensity scale, the scattering length densities (SLD of the core, shell, and

210   solvent), and specific geometric dimensions (length, radius, thickness). To reduce the number of free

211   parameters, the Guinier model was applied in the low-q region of the intensity profile where $q.R_g \leq$

212   1.3, R_g being the radius of gyration of the object. This enabled the determination of R_g and of the

213   intensity scale, the latter being then fixed in the other models. The scattering length density of each

214   molecule was calculated using the SLD calculator of SasView, based on its molecular formula and its

215   mass density. As the assemblies are made of complex mixtures, the exact SLD of core and shells are

216   not known, so the calculated range was used to set initial guesses, letting the values free for the fit,

217   except that of pure water (the solvent), fixed to the calculated value of $9.45.10^{-6}$ Å^{-2} at 20 °C. The SLD

218   initial guess for the core was either set to that of pure water or to an average value of the lipid tails,

219   depending on the model used. The SLD initial guess for the shell was set to an average value for lipid

220   headgroups and surface molecules (bile salt and cholesterol). The radius of gyration was also used for

221 the initial guesses of the geometric dimensions, testing initial aspects ratio of 0.5, 1, and 2 in the

222 cylinder and the ellipsoid models.

223   **3.3.4. Cryo-TEM**

224 Vitrification of samples was performed using an automatic plunge freezer (EM GP, Leica) under

225 controlled humidity and temperature (Dubochet and McDowall, 1981). The samples were deposited

226 on glow-discharged electron microscope grids, followed by blotting and vitrification by rapid freezing

227 into liquid ethane. Grids were transferred to a single-axis cryo-holder (model 626, Gatan) and were

228 observed using a 200 kV electron microscope (Tecnai G2 T20 Sphera, FEI) equipped with a 4k × 4k CCD

229 camera (model USC 4000, Gatan). Micrographs were acquired under low electron doses using the

230 camera in binning mode 1 and at a nominal magnification of 29 000x.

231

232   **4. Results**

233   **4.1. Mixed intestinal assemblies**

234   **4.1.1. Dynamic light scattering**

235 Increasing concentration of FA+MG in simple intestinal bile had different effects on the number-based

236 mean diameter (Dn) of the mixed intestinal assemblies depending on the type of lipid added (figure 1).

237 CA+MC concentration had almost no effect on Dn, with an average value of 3.3 ± 0.1 nm for the first

238 sample series (exp1), and of 3.3 ± 0.2 nm for the second sample series (exp2). This was similar to the

239 average value for the SIB samples, of 3.7 ± 0.3 nm. For OA+MO and DHA+MDH, increasing FA+MG

240 concentration resulted in increased assembly diameter, with reproducible values extracted from

241 number-based unimodal distributions up to 8.5 mg mL^{-1}. This point was defined as the transition

242 concentration, above which a steep size increase occurred. This was followed by a transition region

243 between 12 and 26 mg mL^{-1}, with increasing Dn values that were poorly reproducible between

244 independent samples, due to the coexistence of two assembly types (intensity-based distributions

245 became more bimodal, resulting in more polydisperse number-based distributions). Between 29.5 and

246 40 mg mL^{-1}, distributions became less polydisperse again, so Dn values were more reproducible, with

247   average values of 22.8 ± 1.5 nm for OA+MO, and of 19.2 ± 1.8 nm for DHA+MDH. All intensity-based

248   and number-based size distributions for these experiments are given in figure S1.
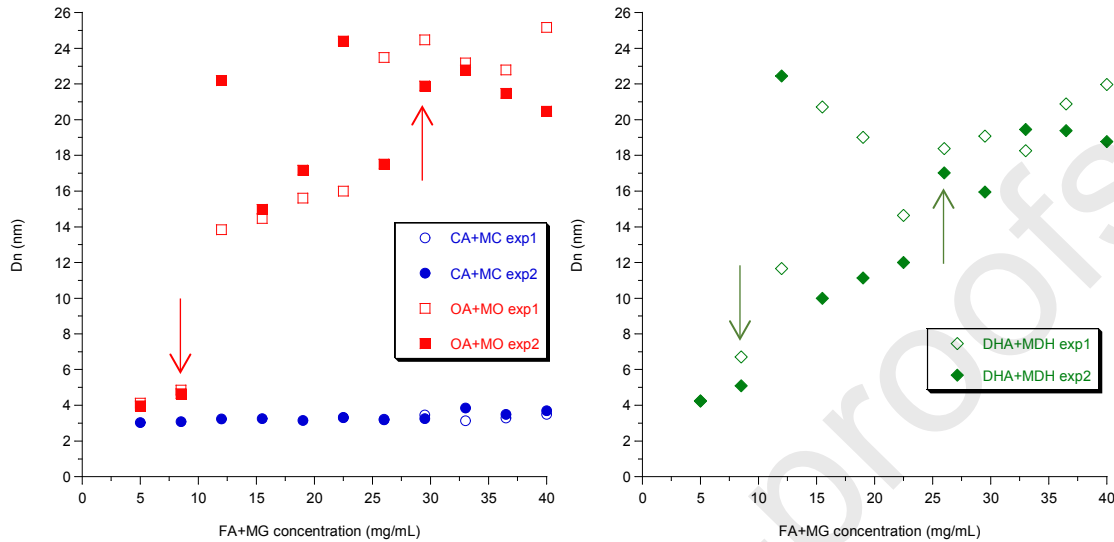
249

250

251   Figure 1: Number-based mean diameter (Dn) of the mixed intestinal assemblies determined by DLS, as a function

252   of FA+MG concentration for each system. Exp1 and exp2 refers to independent sample series preparation and

253   characterization. The arrows indicate the beginning and the end of the transition region.

254

255   **4.1.2.   Turbidimetry**

256   In agreement with the DLS results, sample absorbance (turbidity) did not change significantly with

257   increasing CA+MC concentration, but greatly increased with increasing OA+MO or DHA+MDH

258   concentration (figure 2). For these systems, turbidity increased slightly up to a transition concentration

259   after which it raised abruptly, finishing with a steep increase up to 40 mg mL^{-1}. The transition

260   concentration was either 26 or 22.5 mg mL^{-1} for OA+MO, and was always found to be 26 mg mL^{-1} for

261   DHA+MDH. These values corresponded to the end of the transition region defined with DLS results.
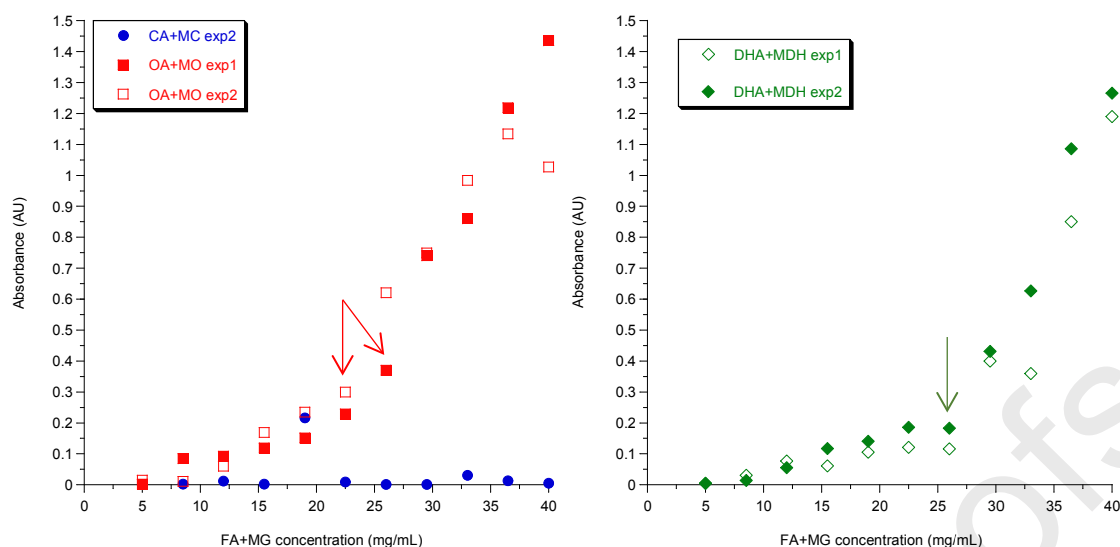
262

263

264 Figure 2: Absorbance of the mixed intestinal assemblies determined by turbidimetry, as a function of FA+MG

265 concentration for each system. Exp1 and exp2 refers to independent sample series preparation and

266 characterization. The arrows indicate the transition concentrations.

267

268 **4.1.3. Small angle X-ray scattering**

269 As DLS results are based on sphere size distribution, giving no indication on the structure and shape of

270 the measured objects, SAXS measurements were performed to characterize these features in the

271 whole FA+MG concentration range. Figure 3 shows representative examples of the intensity profile for

272 the different mixed intestinal assemblies at various FA+MG concentrations, at 20 °C. The effect of

273 temperature was tested for several systems, and no change was observed in the intensity profile in

274 the range 20-60 °C. Overall, each system displayed specific intensity profiles. Those for CA+MC mixed

275 intestinal assemblies were similar within the concentration range, with a broad peak at high q values

276 and a plateau at low q values (with further intensity increase at lower q values in some cases). This

277 broad peak indicated a core-shell structure and the plateau enabled the determination of a small finite

278 size. Such profiles were also observed for OA+MO and DHA+MDH mixed intestinal assemblies up to 8

279 mg mL^{-1}, changing significantly in the transition region defined with DLS results, reaching a final specific

280 profile at 22.5 and 29.5 mg mL^{-1} for OA+MO and DHA+MDH, respectively. These profiles were

281 characterized by a very broad peak centered at lower q values compared to low-concentration profiles,

282 and an upward slope in the lowest q region. Again, a core-shell structure can be presumed, likely

283 polydisperse given the large broadness of the peak. The absence of a low-q plateau indicated a large

284 finite size that is out of the measurement range, and can only be estimated.
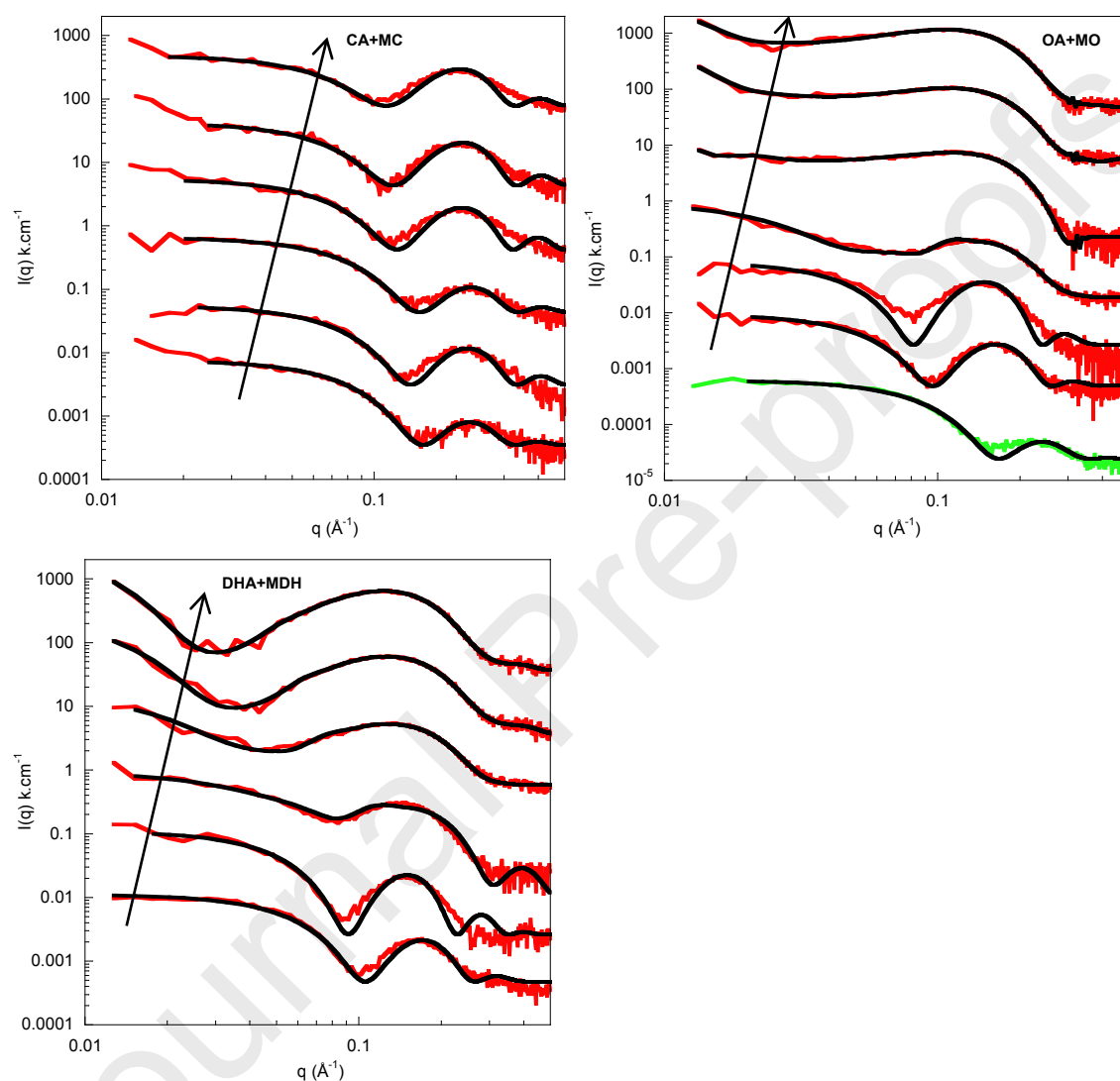
285

286

287

288 Figure 3: Representative SAXS intensity profiles for mixed intestinal assemblies at 20 °C with increasing

289 concentrations (5, 8.5, 15.5, 26, 33, 40 mg mL^{-1}) of CA+MC (top left), OA+MO (top right), or DHA+MDH (bottom).

290 The intensities of successive profiles are shifted by a 10-fold factor, those for the lowest concentration not being

291 shifted. The intensity profile of the SIB, shifted by a 0.1-fold factor, is given in green. The black lines show the fits

292 with the core-multi-shell sphere model.

293

294   To go further and extract morphological features, intensity profiles for the full concentration series

295   were fitted using the three models described in 3.3.3. The core-shell cylinder model did not capture

296   any profile correctly, resulting in low goodness of fit values. The core-shell ellipsoid model was able to

297   fit the profiles with high goodness of fit values, but returned consistent aspect ratio and SLD values

298   only for CA+MC and for the first two OA+MO or DHA+MDH concentrations, i.e. up to the transition

299   concentration defined with DLS results. The best model over the whole FA+MG concentration range

300   was the core-multi-shell sphere, resulting in equivalently high goodness of fit values and returning

301   consistent SLD values. The fits for the core-multi-shell sphere model are shown in figure 3. Specifically,

302   a monodisperse water-core two-shell model (reducing to a lipid core one-shell model as the water core

303   radius was fitted to a zero value) was found to be optimal for CA+MC and at low OA+MO and

304   DHA+MDH concentrations, whereas a polydisperse water-core three-shell model was found to be

305   optimal starting from the middle of the transition region for OA+MO and DHA+MDH (optimal core size

306   polydispersity of 0.5 and 0.25, respectively).

307   To facilitate parameter comparison, the core-multi-shell sphere model was preferred for all systems

308   although it did not perfectly fit some systems at intermediate to high q values (figure 3). Indeed, better

309   fits were obtained at intermediate to high q values with the oblate core-shell ellipsoid model (average

310   aspect ratio of 0.55 ± 0.15) for CA+MC and for the first two OA+MO or DHA+MDH concentrations,

311   indicating deformed spheroids rather than perfect spheres. However, this model was unstable above

312   these first two OA+MO or DHA+MDH concentrations, returning highly variable aspect ratio and SLD

313   values, making it unsuitable for our purpose of studying assembly transition regions. To illustrate these

314   core-shell ellipsoid results, fits for the lowest and highest FA+MG concentrations in all systems are

315   shown in figures S2 and S3.

316   The parameters of the core-multi-shell sphere model are given in table S1 and some geometric

317   dimensions are plotted in figure 4 (parameters of the core-shell ellipsoid model are also given in figures

318   S2 and S3). As seen in table S1, the parameter values were close for duplicate or triplicate samples,

319   indicating reproducible sample preparation. From these data, two types of assembly could be

320   identified: i) lipid-core-shell micelles for CA+MC and at low OA+MO and DHA+MDH concentrations

321   (fitted water core radius of 0 in table S1), ii) water-core vesicle with a three-shell membrane for

322   OA+MO and DHA+MDH at intermediate to high concentrations (figure 4 illustrations). The main

323   transition evidenced in figure 4 for OA+MO and DHA+MDH occured at intermediate concentrations

324   compared to those determined by DLS and turbidimetry. However, in detail, a transition region similar

325   to the one defined with DLS results was identified, in which the external or the internal shell thickness

326   was abnormally thin (table S1). This was an artifact probably due to micelle-vesicle coexistence. The

327   values of the assembly total diameter (D) deduced from the SAXS measurements (figure 4) were

328   systematically 40 ± 3 % larger than those determined by DLS (D_n). These calculated diameters were

329   thus consistently related, although their absolute values differed from one technique to the other.
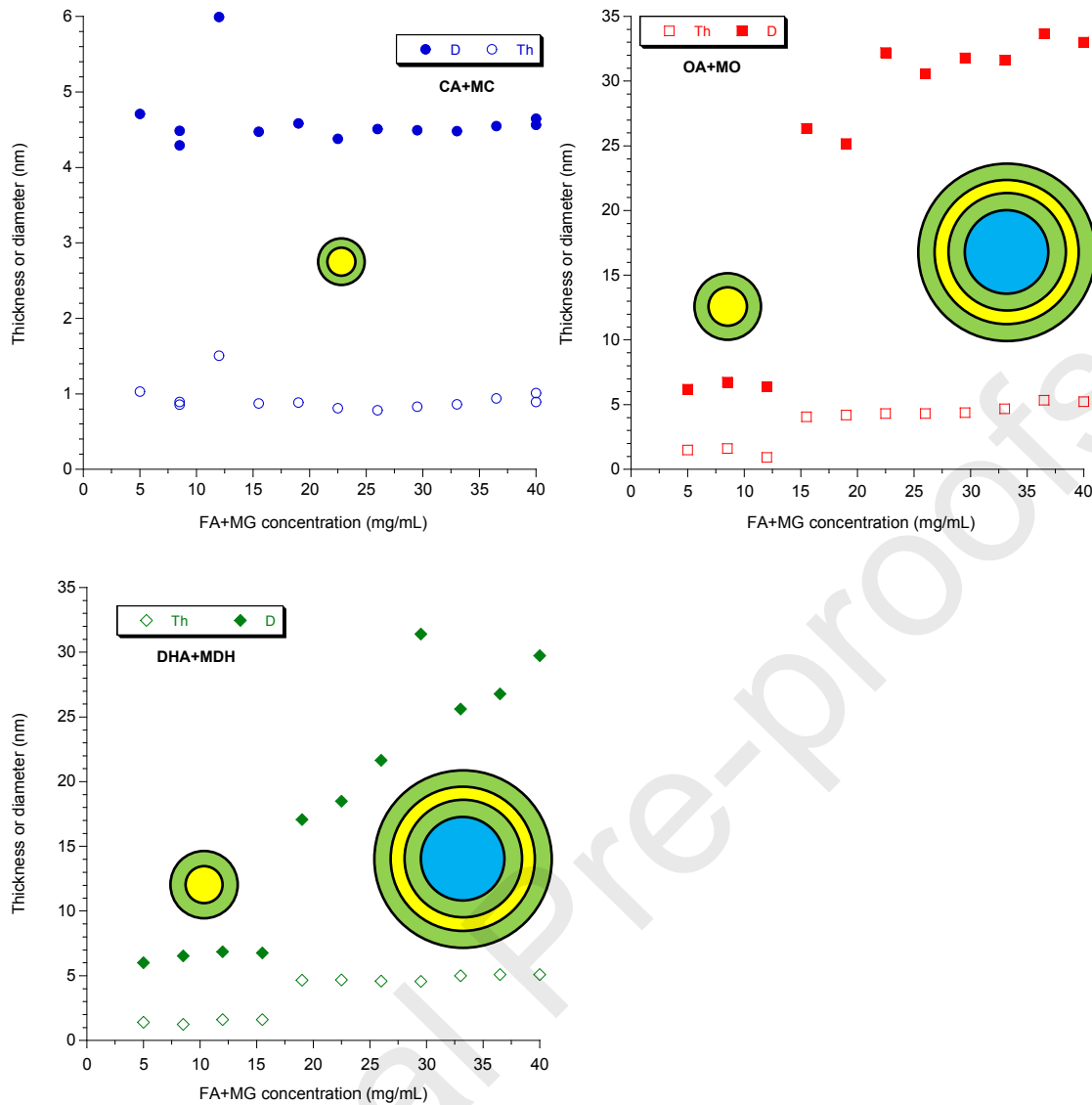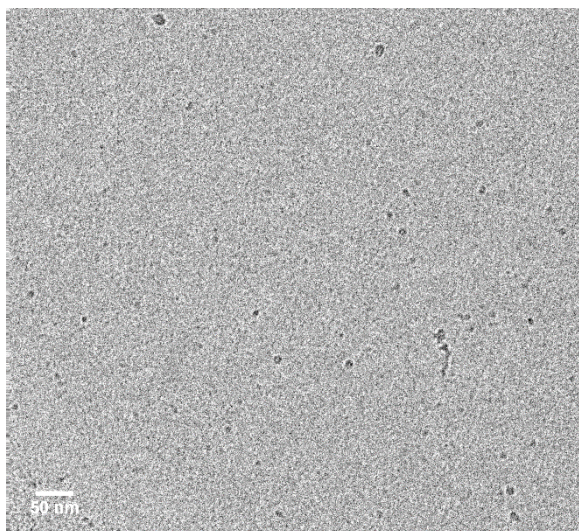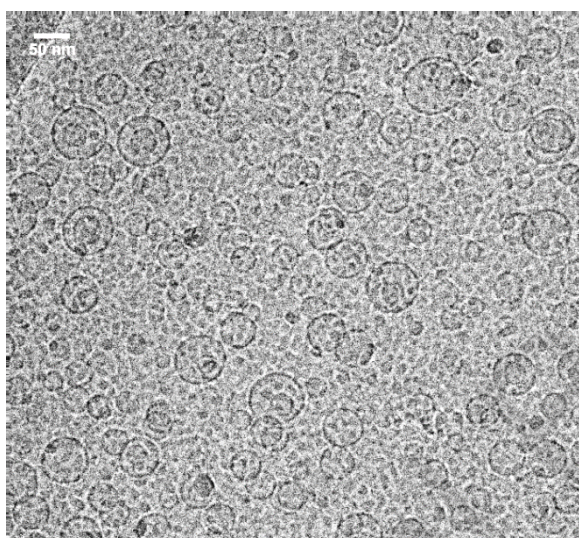
330

331

332

333

334

Figure 4: Main parameters of the core-multi-shell sphere model (total diameter D, and shell thickness Th) for mixed intestinal assemblies containing CA+MC (top left), OA+MO (top right), and DHA+MDH (bottom). Illustrations are drawn to scale, except vesicles for which only the membrane is drawn to scale.
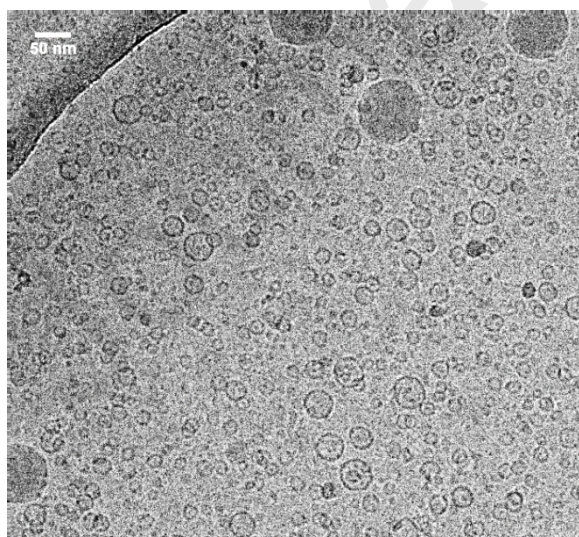
338

339   **4.1.4.   Cryo-TEM**

340

341

342

343

344 Figure 5: Representative cryo-TEM micrographs for OA+MO 5 (OA+MO at 5 mg mL^{-1}, top), OA+MO 40 (OA+MO

345 at 40 mg mL^{-1}, middle), and DHA+MDH 40 (DHA+MDH at 40 mg mL^{-1}, bottom) systems.

346

347   Systems including the lowest and highest FA+MG concentration (denoted FA+MG 5 and FA+MG 40,

348   respectively) were observed under cryo-TEM to check the assemblies and their size. These

349   observations confirmed that OA+MO 40 and DHA+MDH 40 systems contained unilamellar vesicles,

350   ranging from 20 to 60 nm and from 10 to 40 nm, respectively. This also confirmed that vesicles

351   containing OA+MO 40 were larger and more polydisperse than vesicles containing DHA+MDH 40. This

352   was also in agreement with the mean diameters determined by DLS and SAXS, comprised in these

353   ranges. In the OA+MO 40 system, some vesicles above 60 nm contained a smaller vesicle in their

354   internal water phase. These double vesicles (vesicle-in-vesicle) were scarcer in the DHA+MDH 40

355   system, although a few could be observed. For OA+MO 5, dense objects ranging from a few nm to 10

356   nm were observed, in agreement with the DLS and SAXS results. Most of them seemed spherical and

357   a few resembled slightly deformed spheroids, but cryo-TEM resolution was not high enough to

358   investigate their exact morphology.

359

360   **4.2. Vitamin solubilization in mixed intestinal assemblies**

361   Accounting for the above results, two FA+MG concentrations were selected to test fat-soluble vitamin

362   solubilization in unimodal distribution mixed intestinal assemblies of which the geometric dimensions

363   could be accurately characterized. Those were the two extrema: 5 and 40 mg mL^{-1} (denoted FA+MG 5

364   and FA+MG 40).

365   **4.2.1.   Dynamic light scattering**

366   Examples of size measurements as a function of α-tocopherol (VE) concentration in OA+MO mixed

367   intestinal assemblies are reported in figure 6. It shows that Dn at the lowest VE concentration was

368   slightly larger than without VE (see figure 1). Then, it increased or fluctuated with increasing VE

369   concentration in OA+MO 5 or OA+MO 40 systems, respectively. Above a critical VE concentration,

370   there was an abrupt transition of the diameter value, increasing above 100 nm, the number-based size

371   distribution becoming bimodal (Dn was determined for the major peak). We defined this critical

372   concentration as the solubilization capacity, above which the vitamin is not solubilized in the initial

373 assembly anymore. In figure 6, its values were reproducibly of 7.9 and 12.6 mg mL^{-1} in OA+MO 5 and

374 OA+MO 40 systems, respectively. The same experiments were done for the other FA+MG systems, all

375 displaying an abrupt transition at a critical VE concentration. The other vitamins were also tested in all

376 FA+MG systems at 5 and 40 mg mL^{-1}, phylloquinone (VK) and retinol (VA) systems also displaying an

377 abrupt size transition. However, for VA, such a transition was only found in micellar systems, no

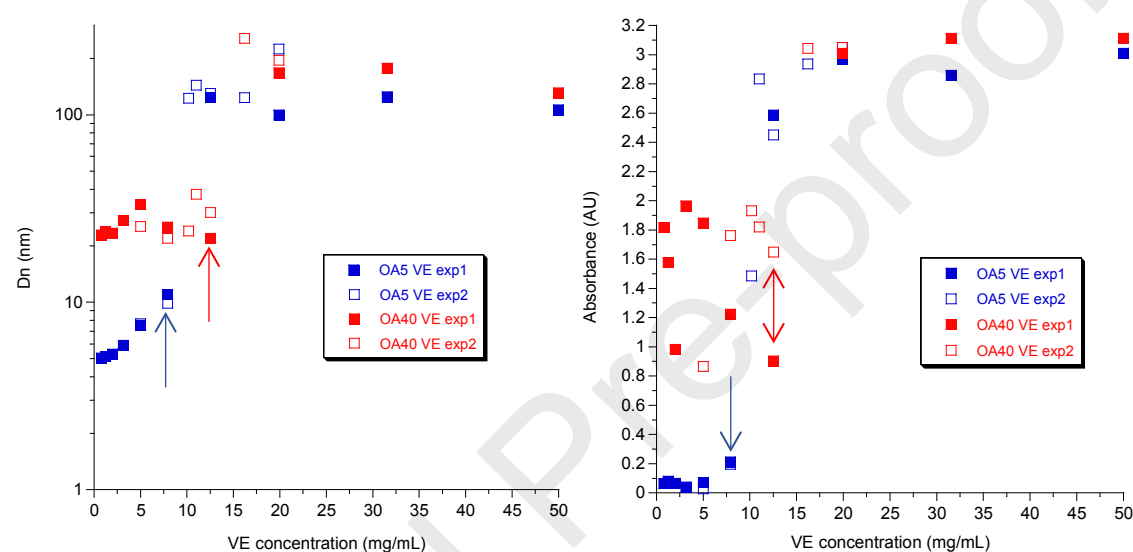378 transition being detected in vesicular systems.

379

380

381 Figure 6: Dn and absorbance of mixed intestinal assemblies as a function of VE concentration in OA+MO 5 or

382 OA+MO 40 systems. The arrows indicate the solubilization capacity.

383

384 The vitamin solubilization capacity ranges determined by DLS are shown in figure 7. The solubilization

385 capacity of the mixed intestinal assemblies depended more on the FA+MG concentration than on the

386 FA+MG type. The solubilization capacity also depended on the vitamin type, higher amounts of VE

387 being solubilized compared to VA and VK (lowest amounts for VK). In all systems, cholecalciferol (VD)

388 addition did not induce any abrupt transition, diameter being constant up to very high concentrations.

389 Only concentrations above 1 mg mL^{-1} resulted in a slight diameter increase.
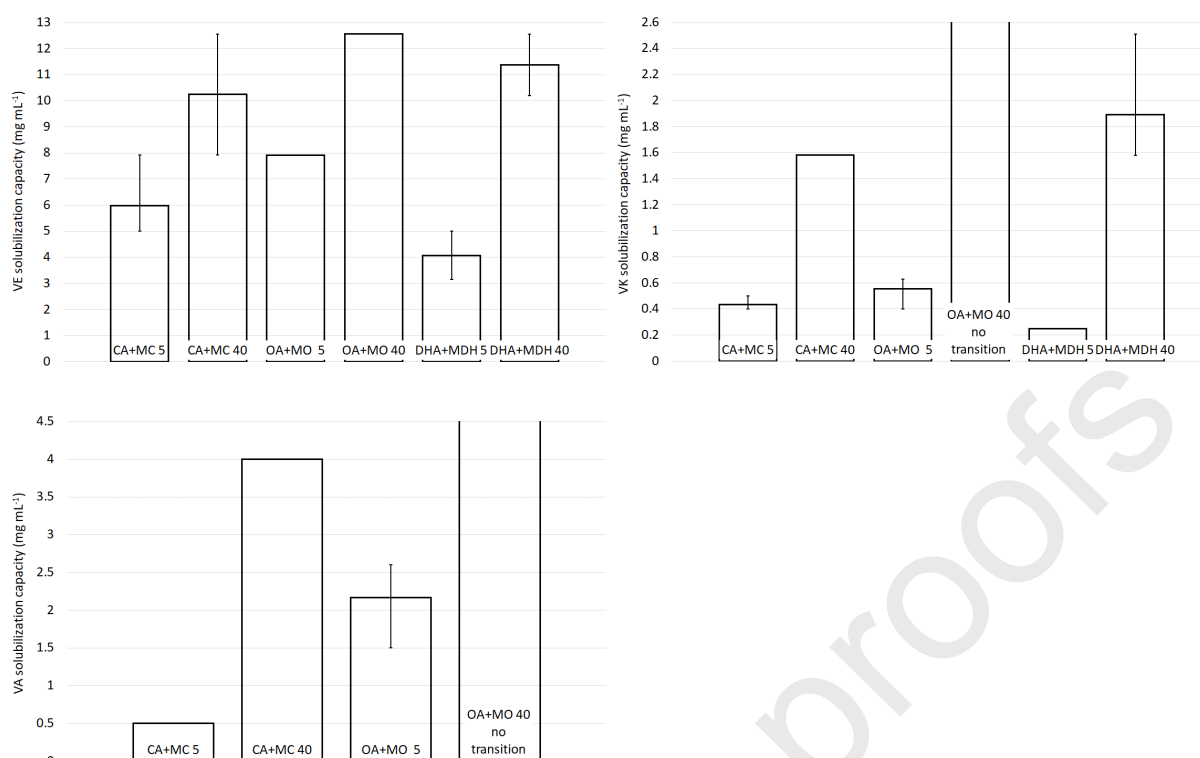
390

391

392

393 Figure 7: Solubilization capacity mean and range for VE (left), VK (right), or VA (bottom) as determined by DLS.

394 When no range appears, values were reproducible (2 to 3 independent samples series). Bars higher than the

395 scale maximum means that no transition was found in the vitamin range investigated.

396

4.2.2. Turbidimetry

398 Mixed intestinal assemblies containing the different vitamins were also analyzed using turbidimetry.

399 The results for the same systems presented above are also shown in figure 6. Similar trends were

400 observed, with abrupt transitions at the same critical concentrations than those determined by DLS.

401 Again, this type of behavior was found for VE, VK, and VA, but not for VD, inducing no abrupt turbidity

402 change within its concentration range (table 3). Overall, the solubilization capacity values determined

403 by turbidimetry were most of the time in agreement with those determined by DLS.

4.2.3. Small angle X-ray scattering

405 Mixed intestinal assemblies containing VE or VK at the solubilization capacity were characterized by

406 SAXS. The concentrations of VD and VA were chosen to correspond to the upper intake (dose) in the

407 mouse, that is 0.14 and 0.2 mg mL^{-1}, respectively. The same models were applied to the intensity

408 profiles (see figures S3), the parameters for the core-multi-shell sphere models being reported in table

409 S2, and the SAXS curves and fits being reported in figures S3. When comparing the geometric

410 dimensions of the mixed intestinal assemblies with or without vitamin, it appeared that only VE had a

411 significant effect on micelles, systematically enlarging them. In contrast, vesicles could be either

412 enlarged or reduced by any vitamin addition except VD, mainly by a modulation of the water core size.

413 **4.2.4. Cryo-TEM**

414 Mixed intestinal assemblies of OA+MO 5 and OA+MO 40 containing VE were also observed by cryo-

415 TEM (figure 8). This confirmed that the addition of VE below the solubilization capacity did not change

416 the structure and apparent size distribution of the assemblies (see figure 5). Note that above 60 nm,

417 double or multiple vesicles also occurred in OA+MO 40 VE 5 samples (VE 5 meaning VE at 5 mg mL^{-1}).
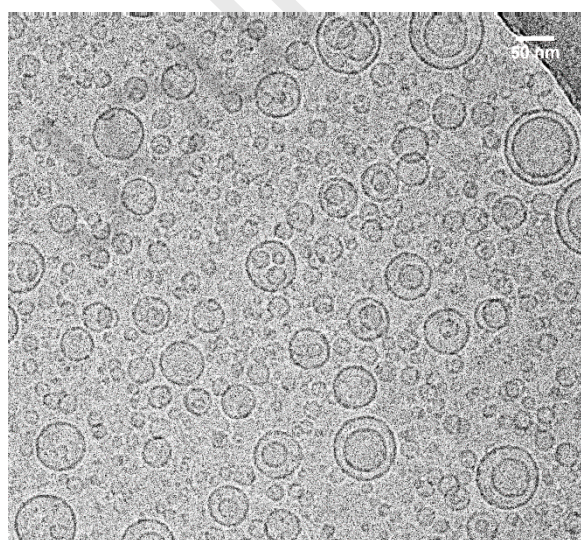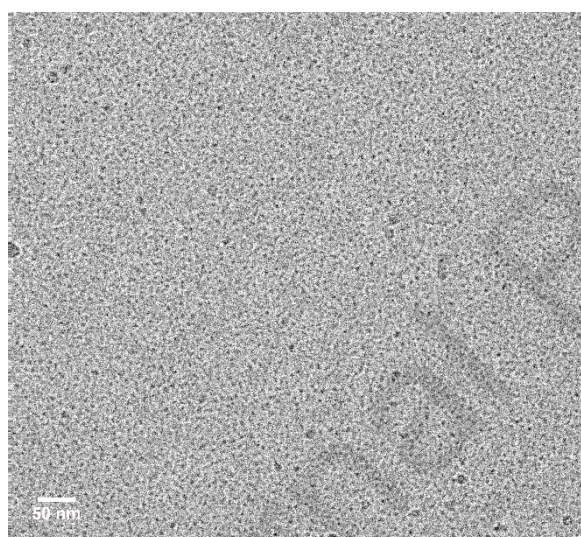

418

419

420 Figure 8: Representative cryo-TEM micrographs for OA+MO 5 VE 3 (VE at 3 mg mL^{-1}, top), and OA+MO 40 VE 5

421 (VE at 5 mg mL^{-1}, bottom) systems.

422

423 **5. Discussion**

424 **5.1. Mixed intestinal assemblies**

425 Size data on mixed intestinal assemblies including lysophospholipid (rather than phospholipid) are

426 scarce, although lysophospholipid is the main phospholipid species in the small intestine (Arnesjo et

427 al., 1969). Additionally, when considering different studies, size values can be difficult to compare as:

428 i) systems are never entirely identical (different concentration, number, and type of components), and

429 ii) DLS size distributions are not interpreted using the same mean value (number-based, volume-based,

430 intensity-based, etc.). Nevertheless, for similar fed-state systems containing at least bile salt,

431 lysophospholipid and OA, the DLS diameter (mean value types not known) of micelles was reported to

432 be 5.7 ± 0.6 nm (Fatouros et al., 2009b) or 5.3 ± 0.5 nm (Birru et al., 2014), only slightly larger than the

433 average value of Dn we obtained at low OA+MO concentrations, of 4.4 ± 0.4 nm (figure 1). For other

434 fed-state systems containing phospholipid, OA, and MO, micelles and vesicles of 33 ± 4 nm and 55 ± 3

435 nm (intensity-based mean diameter, Nielsen et al., 2001), 8.2 nm and 140 nm (number-based mean

436 diameter, Kossena et al., 2003), 5.2 ± 0.2 nm, 27 ± 2 nm and 90 ± 18 nm (volume-based mean diameter,

437 Ilardia-Arana et al., 2006), 5.8 ± 0.5 nm and 67 ± 14 nm (volume-based mean diameter, Kleberg et al.,

438 2010) were reported. The micelle diameters are similar to our values, but the vesicle diameters are

439 always significantly larger than the ones we reported here. In these articles, the 33 nm, 55 nm, and 27

440 nm values were interpreted as mixed micelle diameters, but could more likely correspond to the small

441 vesicles we identified here.

442 We used the same techniques as Birru et al. (2014) and obtained similar behaviors, validating the ability

443 of DLS and turbidimetry to determine structural transitions. However, as their samples were not

444 filtered, mixtures of micelles and very large vesicles (in the range 400-600 nm) were obtained at high

445 lysophospholipid+OA ratios (Birru et al., 2014). In our case, samples were filtered, removing assemblies

446   above 220 nm (as seen in figure 6), in order to normalize preparation and characterize single

447   assemblies (except in the transition regions). In a second study, mixtures of micelles and vesicles were

448   obtained at high OA+MO ratios, with bimodal or trimodal distributions (unfiltered samples), the

449   smallest mean size being about 30 nm (Birru et al., 2017). This size was interpreted as a large micelle

450   diameter, but could again correspond to the small vesicles we identified here. In the first article

451   reporting size transitions using DLS for mixed intestinal assemblies (with a phospholipid, and addition

452   of OA, MO, and DO), an abrupt transition from 6.0 nm micelles to 100 nm vesicles was also observed

453   (Staggers et al., 1990).

454   Overall, the discrepancy in the size values might be due to: i) the use of different distribution types to

455   calculate the mean diameter, ii) measurement difficulties in unfiltered samples containing coexisting

456   assemblies (Kleberg et al., 2010; Birru et al., 2014; 2017), iii) the use of varying lipid/bile salt ratios at

457   a constant total concentration, meaning that bile salt concentration decreases as lipid concentration

458   increases (Staggers et al., 1990; Birru et al., 2014; 2017). In the present study, we used a constant bile

459   salt concentration (constant SIB composition and concentration) and we increased FA+MG

460   concentrations, resulting in transitions only depending on FA+MG concentration. The transition

461   concentrations are thus difficult to compare to previous literature values. However, normalized mass

462   solubilization ratio (SR) values are available for various fatty acids and monoglycerides in bile micelles

463   (Marze, 2014). For CA, a SR of 3.5 was reported, which we did not exceed for CA alone, but that we

464   exceeded for CA+MC, with no size or turbidity change. For OA and MO, SR values of 0.62 and 0.52 were

465   reported, respectively. In our experiments, the pure micellar region exists up to a SR of 0.85 for

466   OA+MO, in reasonable agreement.

467   When comparing the transitions determined by DLS and turbidimetry, the first technique identified

468   well the end of the micelle region whereas the second technique identified well the start of the vesicle

469   region. Thus, these techniques appeared to be complementary, but DLS provides important

470   microscopic features (size distributions, mean sizes). Moreover, turbidity depends on both size and

471 concentration, making it difficult to interpret highly turbid regions, such as the vesicle region where

472 turbidity increases continuously. The same was found by Birru et al. (2014; 2017).

473 SAXS experiments enabled a detailed characterization of the assembly structures. A transition from

474 ellipsoidal micelles to spherical vesicles upon OA+MO or DHA+MDH addition was found in the current

475 study. Although this does not agree with some previous studies reporting disk-like shape for fed-state

476 intestinal micelles (Elvang et al., 2016; 2018; 2019; Hernell et al., 1990), this is consistent with other

477 studies reporting spherical (Phan et al., 2015) or ellipsoidal shapes (Clulow et al., 2017; Rezhdo et al.,

478 2017) for fed-state intestinal micelles. More precisely, the geometric diameters of our core-shell oblate

479 ellipsoid micelles (7.0 ± 0.5 nm; 3.6 ± 0.8 nm) are in good agreement with the core-shell oblate ellipsoid

480 micelles of Clulow et al. (6.6 ± 0.1 nm; 4.1 ± 0.1 nm) and the oblate ellipsoid micelles of Rezhdo et al.

481 (6.4 ± 0.6 nm; 3.7 ± 0.1 nm). Upon OA+MO addition, Clulow et al. (2017) reported an increase in the

482 micelle size, and the appearance of another assembly around 26 nm (volume-based mean diameter).

483 This size was interpreted as that for aggregated micelles, but could again correspond to the small

484 vesicles we identified. Vesicles of similar size were indeed found in their fasted state system (modelled

485 as core-multi-shell spheres). Moreover, such small vesicles (intensity-based mean diameter of 25-50

486 nm) were also reported for bile salt+phospholipid systems at low salt concentration and high dilution

487 (Leng et al., 2003). Concerning the vesicle membrane thickness, the values deduced from SAXS

488 measurements (5.1 ± 0.1 nm, table S2) are in very good agreement with the value of 5.2 nm deduced

489 from SAXS measurements of a fed-state OA+MO system (Salentinig et al., 2011).

490 Our cryo-TEM observations confirmed that the systems at the highest OA+MO or DHA+MDH

491 concentration are made of small vesicles. For similar systems containing OA+MO and phospholipid,

492 Fatouros et al. (2009a), using cryo-TEM, also observed small vesicles (below 40-50 nm) and large

493 double or multiple vesicles (above 100 nm). When the phospholipid was replaced by a

494 lysophospholipid, similar assemblies were observed (Fatouros et al., 2009b). After triolein in vitro

495 digestion, Salentinig et al. (2011) also reported that digestion products (OA+MO) associated with bile

496 salts and lysophospholipid to form small unilamellar vesicles (below 50 nm, as observed by cryo-TEM).

497 Finally, Riethorst et al. (2016) used different microscopy techniques to investigate human duodenal

498 fluid collected in the fed state, observing a mixture of micelles, vesicles, and droplets, vesicles being

499 predominant. Vesicle size distribution was large, ranging from 10 to 500 nm, again with small

500 unilamellar vesicles and large multiple vesicles.

501

502 **5.2. Vitamin solubilization in mixed intestinal assemblies**

503 Concerning the techniques to determine solubilization capacity, both DLS and turbidimetry were used

504 before to monitor the solubilization in synthetic surfactant solutions of lipophilic compounds (essential

505 oil components, vitamins) at increasing concentrations. Similar DLS curves with a steep transition were

506 obtained, assemblies being about 100 nm or even more above the transition (Rao and McClements,

507 2012; Ziani et al., 2012). Turbidimetry alone was used in the context of VE solubilization in mixed bile

508 micelles, a transition being also evidenced (Yang and McClements, 2013). Although most of our

509 turbidimetry results were in agreement with our DLS results, this was not always the case. Moreover,

510 transitions can be difficult to identify when a continuous turbidity increase is observed (Rao and

511 McClements, 2012; Ziani et al., 2012). Thus, we consider DLS more relevant for vitamin solubilization

512 studies as it enables the precise determination of successive characteristic sizes in the system

513 depending on vitamin concentration, making it possible to define a solubilization capacity in a specific

514 assembly.

515 To understand the differences in solubilization capacity for the vitamins, we compared the mass

516 solubilization ratios (SR) determined by DLS to those reported in the literature. For VE, our average SR

517 range was from 0.41 to 1.26, which is higher than the literature ranges of 0.14-0.33 (Nielsen et al.,

518 2001) and 0.1-0.2 (Yang and McClements, 2013) in similar conditions but at lower FA and/or MG

519 concentrations, and 0.1-0.2 in low-concentration taurocholate or taurocholate-phosphatidylcholine

520 (Imai et al., 1983). This discrepancy is likely due to much higher FA+MG concentrations in our systems.

521 It was indeed shown that high FA+MG concentrations greatly enhanced drug solubilization (Kossena

522 et al., 2003; 2004; Kleberg et al., 2010).

523 For VK, our average SR range was from 0.025 to 0.19, which is close to the range reported before, from

524 0.02 to 0.25 in high-concentration cholate or cholate-phosphatidylcholine (Nagata et al., 1988). For

525 VA, our average SR range was from 0.05 to 0.4, which is higher than the literature values of 0.002 for

526 retinol in similar conditions but at lower FA+MG concentration (El-Gorab and Underwood, 1973) and

527 0.02 for retinyl palmitate in similar mixtures but in fasted state conditions (Desmarchelier et al., 2018).

528 This could be due to our higher FA+MG concentrations again. Assembly filtration could also explain the

529 difference, as it was shown to retain a large proportion of retinyl palmitate, resulting in an apparent

530 lower solubilization capacity (Desmarchelier et al., 2018). We checked this in our conditions, and no

531 significant effect of the filtrations was found on VA concentration in the assemblies within the

532 concentration range studied, possibly because we used retinol rather than retinyl palmitate. Another

533 critical aspect is vitamin degradation during assembly preparation, which is rarely reported in the

534 literature. For an unmeasured high vitamin degradation, the solubilization capacity will indeed appear

535 higher. As retinol was the most unstable vitamin we investigated, validation experiments were

536 conducted in assemblies containing this molecule compared to the same assemblies containing α-

537 tocopherol. This showed that VA can be degraded up to 50 % after 12 hours (VE was not significantly

538 degraded in the assemblies after 24 hours). Once samples containing VA were prepared on ice,

539 degradation was kept within 10-20 % after 12 hours. When investigating the solubilization capacity, it

540 is thus important to work within 12-24 hours to limit degradation, and even better to quantify
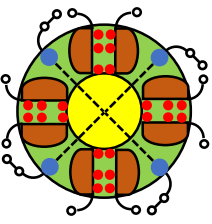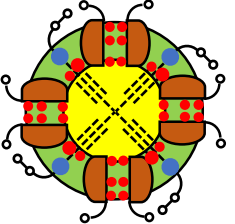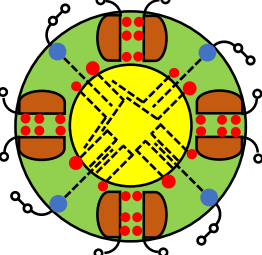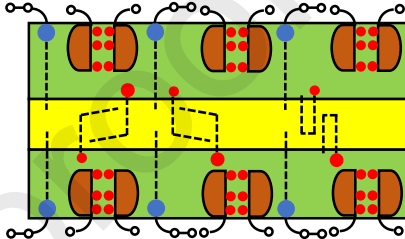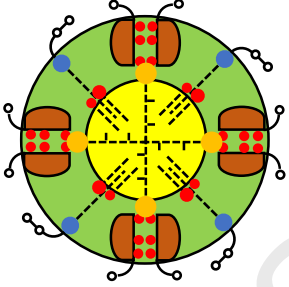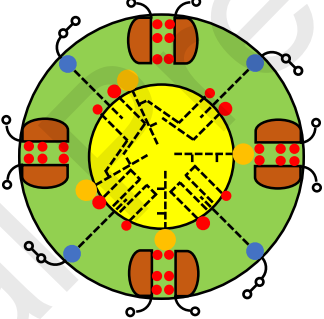
541 degradation.
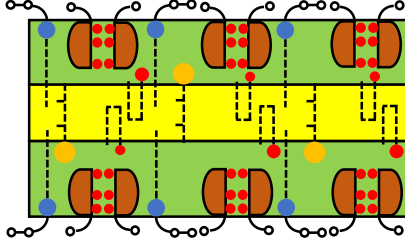
542 For VD, no steep assembly transition was observed, although SR values up to 0.3 were investigated, at

543 least 2-fold higher than those previously studied (Goncalves et al., 2011; Desmarchelier et al., 2018).

544 It was recently shown that cholecalciferol could self-assemble alone in water, thus able to solubilize in

545 the absence of other amphiphilic molecule (Desmarchelier et al., 2018). This might explain why we did

546 not observe any significant assembly change up to high VD concentrations (human nutrition range),

547 VD not being incorporated in mixed intestinal assemblies but forming self-assemblies on its own. We

548 checked this possibility by DLS for 0.14 mg mL^{-1} VD alone in PBS, and found a Dn of 93 ± 11 nm, in

549 agreement with the size range observed by Desmarchelier et al. (2018) using cryo-TEM. However, this

550 size was not detected in any mixed intestinal assembly system containing 0.14 mg mL^{-1} VD, and the

551 SAXS intensity profiles did not change either with 0.14 mg mL^{-1} VD addition. This might be due to the

552 small amount of VD relative to the other components in the systems, too small to be detected as self-

553 assemblies and not inducing any structural change of the mixed intestinal assemblies.

554 As already discussed, any size change or abrupt transition upon vitamin incorporation should be

555 reported, as these changes modify the interpretation of vitamin solubilization. Up to now, only one

556 article dealing with similar systems reported sizes at the solubilization capacity, proving that the

557 assembly size did not change upon α-tocopherol incorporation (Nielsen et al., 2001). This is even more

558 critical since most research groups used the excess vitamin method (addition of vitamin in large excess

559 of the assembly solubilization capacity, then removal of the excess), very likely to induce a change in

560 the size and structure of the solubilizing assembly. In this regard, the techniques we used here

561 (turbidimetry and especially DLS) were more suitable, as vitamin was added gradually in the solubilizing

562 assembly (from below the solubilization capacity).

563 Finally, the supramolecular structure characterization from SAXS enabled reasonable assumptions on

564 vitamin localization in the assemblies. From the geometric dimensions and conformation of the most

565 abundant and most constraining species, plus the comparison of the SLD values of individual species

566 and those of the regions deduced from SAXS sphere models, ideal molecular organizations can be

567 proposed. These are summed up in figure 9. Note that these organizations are only relevant for the

568 localization of the molecules in the different regions (lipid tails region and headgroups/surface

569 molecules region), not for their relative arrangement and amounts. The molecules taken into account

570 were the bile salt dimer (Mazer et al., 1980; Mazer and Carey, 1983), the saturated carbon chain

571 lysophospholipid (longest straight chain and large headgroup), CA and MC (straight chain), OA and MO

572 (bent chain due to the double bond, cf. Rich, 1993), DHA and MDH (folded structure due to the six

573 double bonds, cf. Albrand et al., 1994), and α-tocopherol (straight chain, cf. Setiadi et al., 2003). As

574   seen in figure 9, these molecules match most of the characteristic lengths of the assemblies, validating

575   the assembly core-shell structures and sizes at the molecular scale.

	SIB	CA+MC 5 or CA+MC 40	OA+MO 5 or DHA+MDH 5	OA+MO 40 or DHA+MDH 40
Assemblies alone				
Assemblies with VE				

576

Figure 9: Molecular organization of assemblies inferred from SAXS measurements and models, plus molecular geometric dimensions and conformations. Headgroups/surface molecules region is green, lipid tails region is yellow, TC dimer is brown and red, 16:0 LPC polar head is blue, FA and MG polar heads are red, and VE (α-tocopherol) polar head is orange. All dimensions are to scale. Only a portion of the vesicle membrane is drawn for OA+MO 40 or DHA+MDH 40. When OA+MO and DHA+MDH are drawn in the same assembly, assembly dimensions are not significantly different (only OA+MO 40 VE and DHA+MDH 40 VE are significantly different).

581

582

583   **6. Conclusion**

584 In this study, DLS was found to be the most appropriate method to monitor size transitions of bile

585 intestinal assemblies upon addition of FA+MG and fat-soluble vitamins. The solubilization capacities in

586 assemblies of specific structure could indeed be determined from DLS measurements. SAXS and cryo-

587 TEM experiments complemented these results by revealing the supramolecular structure of these

588 assemblies, i.e. core-shell micelles at low FA+MG concentrations and unilamellar vesicles at high

589 FA+MG concentrations (except with caprylate FA+MG, always yielding micelles). Moreover, SAXS data

590 allowed ideal molecular organizations to be proposed.

591 For the first time, we showed that the incorporation of a fat-soluble vitamin in these micelles and

592 vesicles either induced a systematic structural transition (α-tocopherol VE, phylloquinone VK), or

593 induced a structural transition only for micelles (retinol VA), or no transition at all (cholecalciferol VD).

594 So, confirming our hypothesis, the type and concentration of FA+MG clearly influenced both the

595 structure of the assembly and its solubilization capacity for most of the fat-soluble vitamins studied.

596 Our systematic investigation provides important new solubilization and structure data in many

597 conditions, and proves that structural changes induced by a solubilizate should always be considered

598 to correctly determine the solubilization capacity in a specific assembly. The precise structures above

599 the solubilization capacity should also be characterized in future studies. Thus, our approach and

600 results fill gaps in both methodology and knowledge of mixed intestinal assemblies structure and

601 vitamin solubilization in the fed state, interesting for many applications (colloid science, nutrition,

602 pharmacology, toxicology). More experimental works together with dynamic molecular simulations

603 are currently performed to understand the molecular determinants of these results. In vivo

604 experiments in the mouse are also conducted to determine the role of the intestinal assembly

605 structure on fat-soluble vitamin absorption in the context of nutrition.

606

609

610 **References**

611 Agellon LB, Walkey CJ, Vance DE, Kuipers F, Verkade HJ. 1999. The unique acyl chain specificity of biliary
612   phosphatidylcholines in mice is independent of their biosynthetic origin in the liver.
613   *Hepatology* 30:725-9

614 Albrand M, Pageaux JF, Lagarde M, Dolmazon R. 1994. CONFORMATIONAL-ANALYSIS OF ISOLATED
615   DOCOSAHEXAENOIC ACID (22/6 N-3) AND ITS 14-(S) AND 11-(S) HYDROXY DERIVATIVES BY
616   FORCE-FIELD CALCULATIONS. *Chemistry and Physics of Lipids* 72:7-17

617 Arnesjo B, Nilsson A, Barrowman J, Borgstrom B. 1969. INTESTINAL DIGESTION AND ABSORPTION OF
618   CHOLESTEROL AND LECITHIN IN HUMAN - INTUBATION STUDIES WITH A FAT-SOLUBLE
619   REFERENCE SUBSTANCE. *Scandinavian Journal of Gastroenterology* 4:653-+

620 Baghdasaryan A, Fuchs CD, Osterreicher CH, Lemberger UJ, Halilbasic E, et al. 2016. Inhibition of
621   intestinal bile acid absorption improves cholestatic liver and bile duct injury in a mouse model
622   of sclerosing cholangitis. *Journal of Hepatology* 64:674-81

623 Bizien T, Ameline JC, Yager KG, Marchi V, Artzner F. 2015. Self-Organization of Quantum Rods Induced
624   by Lipid Membrane Corrugations. *Langmuir* 31:12148-54

625 Birru WA, Warren DB, Han SF, Benameur H, Porter CJH, et al. 2017. Computational Models of the
626   Gastrointestinal Environment. 2. Phase Behavior and Drug Solubilization Capacity of a Type I
627   Lipid-Based Drug Formulation after Digestion. *Molecular Pharmaceutics* 14:580-92

628 Birru WA, Warren DB, Ibrahim A, Williams HD, Benameur H, et al. 2014. Digestion of Phospholipids
629   after Secretion of Bile into the Duodenum Changes the Phase Behavior of Bile Components.
630   *Molecular Pharmaceutics* 11:2825-34

631 Boquillon M, Clement J. 1979. EFFECT OF TYPE AND AMOUNT OF DIETARY-FAT ON BILE-FLOW AND
632   COMPOSITION IN RATS. *Annales De Biologie Animale Biochimie Biophysique* 19:1725-36

633 Carey MC, Small DM. 1970. CHARACTERISTICS OF MIXED MICELLAR SOLUTIONS WITH PARTICULAR
634   REFERENCE TO BILE. *American Journal of Medicine* 49:590-&

635 Clulow AJ, Parrow A, Hawley A, Khan J, Pham AC, et al. 2017. Characterization of Solubilizing
636   Nanoaggregates Present in Different Versions of Simulated Intestinal Fluid. *Journal of Physical*
637   *Chemistry B* 121:10869-81

638 Cohen DE, Thurston GM, Chamberlin RA, Benedek GB, Carey MC. 1998. Laser light scattering evidence
639   for a common wormlike growth structure of mixed micelles in bile salt- and straight-chain
640   detergent-phosphatidylcholine aqueous systems: Relevance to the micellar structure of bile.
641   *Biochemistry* 37:14798-814

642 Desmarchelier C, Rosilio V, Chapron D, Makky A, Preveraud DP, et al. 2018. Molecular interactions

643 governing the incorporation of cholecalciferol and retinyl-palmitate in mixed taurocholate-
644 lipid micelles. *Food Chemistry* 250:221-9

645 Dubochet J, McDowall AW. 1981. VITRIFICATION OF PURE WATER FOR ELECTRON-MICROSCOPY.
646 *Journal of Microscopy-Oxford* 124:RP3-RP4

647 Egelhaaf SU, Schurtenberger P. 1999. Micelle-to-vesicle transition: A time-resolved structural study.
648 *Physical Review Letters* 82:2804-7

649 El-Gorab M, Underwood BA. 1973. SOLUBILIZATION OF BETA-CAROTENE AND RETINOL INTO
650 AQUEOUS-SOLUTIONS OF MIXED MICELLES. *Biochimica Et Biophysica Acta* 306:58-66

651 Elvang PA, Bohsen MS, Stein PC, Bauer-Brandl A, Riethorst D, et al. 2019. Co-existing colloidal phases
652 of human duodenal aspirates: Intraindividual fluctuations and interindividual variability in
653 relation to molecular composition. *Journal of Pharmaceutical and Biomedical Analysis* 170:22-
654 9

655 Elvang PA, Hinna AH, Brouwers J, Hens B, Augustijns P, Brandl M. 2016. Bile Salt Micelles and
656 Phospholipid Vesicles Present in Simulated and Human Intestinal Fluids: Structural Analysis by
657 Flow FieldeFlow Fractionation/Multiangle Laser Light Scattering. *Journal of Pharmaceutical*
658 *Sciences* 105:2832-9

659 Elvang PA, Jacobsen AC, Bauer-Brandl A, Stein PC, Brandl M. 2018. Co-existing colloidal phases in
660 artificial intestinal fluids assessed by AF4/MALLS and DLS: A systematic study into cholate &
661 (lyso-) phospholipid blends, incorporating celecoxib as a model drug. *European Journal of*
662 *Pharmaceutical Sciences* 120:61-72

663 Fatouros DG, Walrand I, Bergenstahl B, Mullertz A. 2009. Colloidal Structures in Media Simulating
664 Intestinal Fed State Conditions with and Without Lipolysis Products. *Pharmaceutical Research*
665 26:361-74

666 Fatouros DG, Walrand I, Bergenstahl B, Mullertz A. 2009. Physicochemical Characterization of
667 Simulated Intestinal Fed-State Fluids Containing Lyso-Phosphatidylcholine and Cholesterol.
668 *Dissolution Technologies* 16:47-50

669 Goncalves A, Gleize B, Bott R, Nowicki M, Amiot MJ, et al. 2011. Phytosterols can impair vitamin D
670 intestinal absorption in vitro and in mice. *Molecular Nutrition & Food Research* 55:S303-S11

671 Grundy SM, Metzger AL. 1972. PHYSIOLOGICAL METHOD FOR ESTIMATION OF HEPATIC SECRETION OF
672 BILIARY LIPIDS IN MAN. *Gastroenterology* 62:1200-&

673 Hernell O, Staggers JE, Carey MC. 1990. PHYSICAL-CHEMICAL BEHAVIOR OF DIETARY AND BILIARY
674 LIPIDS DURING INTESTINAL DIGESTION AND ABSORPTION .2. PHASE-ANALYSIS AND
675 AGGREGATION STATES OF LUMINAL LIPIDS DURING DUODENAL FAT DIGESTION IN HEALTHY
676 ADULT HUMAN-BEINGS. *Biochemistry* 29:2041-56

677 Hjelm RP, Thiyagarajan P, Alkanonyuksel H. 1992. ORGANIZATION OF PHOSPHATIDYLCHOLINE AND

678   BILE-SALT IN RODLIKE MIXED MICELLES. *Journal of Physical Chemistry* 96:8653-61

679 Ilardia-Arana D, Kristensen HG, Mullertz A. 2006. Biorelevant dissolution media: Aggregation of
680   amphiphiles and solubility of estradiol. *Journal of Pharmaceutical Sciences* 95:248-55

681 Imai J, Hayashi M, Awazu S, Hanano M. 1983. SOLUBILIZATION OF DL-ALPHA-TOCOPHEROL BY BILE-
682   SALTS, POLYSORBATE-80 AND EGG LECITHIN. *Chemical & Pharmaceutical Bulletin* 31:4077-82

683 Juste C, Demarne Y, Corring T. 1983. RESPONSE OF BILE-FLOW, BILIARY LIPIDS AND BILE-ACID POOL IN
684   THE PIG TO QUANTITATIVE VARIATIONS IN DIETARY-FAT. *Journal of Nutrition* 113:1691-701

685 Kleberg K, Jacobsen F, Fatouros DG, Mullertz A. 2010. Biorelevant Media Simulating Fed State Intestinal
686   Fluids: Colloid Phase Characterization and Impact on Solubilization Capacity. *Journal of*
687   *Pharmaceutical Sciences* 99:3522-32

688 Kok T, Hulzebos CV, Wolters H, Havinga R, Agellon LB, et al. 2003. Enterohepatic circulation of bile salts
689   in farnesoid x receptor-deficient mice - Efficient intestinal bile salt absorption in the absence
690   of ileal bile acid-binding protein. *Journal of Biological Chemistry* 278:41930-7

691 Kossena GA, Boyd BJ, Porter CJH, Charman WN. 2003. Separation and characterization of the colloidal
692   phases produced on digestion of common formulation lipids and assessment of their impact
693   on the apparent solubility of selected poorly water-soluble drugs. *Journal of Pharmaceutical*
694   *Sciences* 92:634-48

695 Kossena GA, Charman WN, Boyd BJ, Dunstan DE, Porter CJH. 2004. Probing drug solubilization patterns
696   in the gastrointestinal tract after administration of lipid-based delivery systems: A phase
697   diagram approach. *Journal of Pharmaceutical Sciences* 93:332-48

698 Leng J, Egelhaaf SU, Cates ME. 2003. Kinetics of the micelle-to-vesicle transition: Aqueous lecithin-bile
699   salt mixtures. *Biophysical Journal* 85:1624-46

700 Madenci D, Salonen A, Schurtenberger P, Pedersen JS, Egelhaaf SU. 2011. Simple model for the growth
701   behaviour of mixed lecithin-bile salt micelles. *Physical Chemistry Chemical Physics* 13:3171-8

702 Marze S. 2014. A coarse-grained simulation to study the digestion and bioaccessibility of lipophilic
703   nutrients and micronutrients in emulsion. *Food & Function* 5:129-39

704 Mazer NA, Benedek GB, Carey MC. 1980. QUASI-ELASTIC LIGHT-SCATTERING-STUDIES OF AQUEOUS
705   BILIARY LIPID SYSTEMS - MIXED MICELLE FORMATION IN BILE-SALT LECITHIN SOLUTIONS.
706   *Biochemistry* 19:601-15

707 Mazer NA, Carey MC. 1983. QUASI-ELASTIC LIGHT-SCATTERING-STUDIES OF AQUEOUS BILIARY LIPID
708   SYSTEMS - CHOLESTEROL SOLUBILIZATION AND PRECIPITATION IN MODEL BILE SOLUTIONS.
709   *Biochemistry* 22:426-42

710 Muller K. 1981. STRUCTURAL DIMORPHISM OF BILE-SALT LECITHIN MIXED MICELLES - A POSSIBLE
711   REGULATORY MECHANISM FOR CHOLESTEROL SOLUBILITY IN BILE - X-RAY STRUCTURE-
712   ANALYSIS. *Biochemistry* 20:404-14

713 Nagata M, Yotsuyanagi T, Ikeda K. 1988. SOLUBILIZATION OF VITAMIN-K1 BY BILE-SALTS AND
714   PHOSPHATIDYLCHOLINE-BILE SALTS MIXED MICELLES. *Journal of Pharmacy and Pharmacology*
715   40:85-8

716 Nichols JW, Ozarowski J. 1990. SIZING OF LECITHIN-BILE SALT MIXED MICELLES BY SIZE-EXCLUSION
717   HIGH-PERFORMANCE LIQUID-CHROMATOGRAPHY. *Biochemistry* 29:4600-6

718 Nielsen PB, Mullertz A, Norling T, Kristensen HG. 2001. The effect of alpha-tocopherol on the in vitro
719   solubilisation of lipophilic drugs. *International Journal of Pharmaceutics* 222:217-24

720 Pathak P, Xie C, Nichols RG, Ferrell JM, Boehme S, et al. 2018. Intestine farnesoid X receptor agonist
721   and the gut microbiota activate G-protein bile acid receptor-1 signaling to improve
722   metabolism. *Hepatology* 68:1574-88

723 Phan S, Salentinig S, Gilbert E, Darwish TA, Hawley A, et al. 2015. Disposition and crystallization of
724   saturated fatty acid in mixed micelles of relevance to lipid digestion. *Journal of Colloid and*
725   *Interface Science* 449:160-6

726 Rao JJ, McClements DJ. 2012. Lemon oil solubilization in mixed surfactant solutions: Rationalizing
727   microemulsion & nanoemulsion formation. *Food Hydrocolloids* 26:268-76

728 Reeves PG, Nielsen FH, Fahey GC. 1993. AIN-93 PURIFIED DIETS FOR LABORATORY RODENTS - FINAL
729   REPORT OF THE AMERICAN INSTITUTE OF NUTRITION AD HOC WRITING COMMITTEE ON THE
730   REFORMULATION OF THE AIN-76A RODENT DIET. *Journal of Nutrition* 123:1939-51

731 Rezhdo O, Di Maio S, Le P, Littrell KC, Carrier RL, Chen SH. 2017. Characterization of colloidal structures
732   during intestinal lipolysis using small-angle neutron scattering. *Journal of Colloid and Interface*
733   *Science* 499:189-201

734 Rich MR. 1993. CONFORMATIONAL-ANALYSIS OF ARACHIDONIC AND RELATED FATTY-ACIDS USING
735   MOLECULAR-DYNAMICS SIMULATIONS. *Biochimica Et Biophysica Acta* 1178:87-96

736 Riethorst D, Baatsen P, Remijn C, Mitra A, Tack J, et al. 2016. An In-Depth View into Human Intestinal
737   Fluid Colloids: Intersubject Variability in Relation to Composition. *Molecular Pharmaceutics*
738   13:3484-93

739 Salentinig S, Sagalowicz L, Leser ME, Tedeschi C, Glatter O. 2011. Transitions in the internal structure
740   of lipid droplets during fat digestion. *Soft Matter* 7:650-61

741 SasView website: https://www.sasview.org

742 Schurtenberger P, Mazer N, Kanzig W. 1985. MICELLE TO VESICLE TRANSITION IN AQUEOUS-
743   SOLUTIONS OF BILE-SALT AND LECITHIN. *Journal of Physical Chemistry* 89:1042-9

744 Setiadi DH, Chass GA, Koo JCP, Penke B, Csizmadia IG. 2003. Exploratory study on the full conformation
745   space of alpha-tocopherol and its selected congeners. *Journal of Molecular Structure-*
746   *Theochem* 666:439-43

747 Small DM, Penkett SA, Chapman D. 1969. STUDIES ON SIMPLE AND MIXED BILE SALT MICELLES BY

748   NUCLEAR MAGNETIC RESONANCE SPECTROSCOPY. *Biochimica Et Biophysica Acta* 176:178-&

749 Staggers JE, Hernell O, Stafford RJ, Carey MC. 1990. PHYSICAL-CHEMICAL BEHAVIOR OF DIETARY AND

750   BILIARY LIPIDS DURING INTESTINAL DIGESTION AND ABSORPTION .1. PHASE-BEHAVIOR AND

751   AGGREGATION STATES OF MODEL LIPID SYSTEMS PATTERNED AFTER AQUEOUS DUODENAL

752   CONTENTS OF HEALTHY ADULT HUMAN-BEINGS. *Biochemistry* 29:2028-40

753 Sugano M, Watanabe M, Kohno M, Cho YJ, Ide T. 1983. EFFECTS OF DIETARY TRANS-FAT ON BILIARY

754   AND FECAL STEROID-EXCRETION AND SERUM-LIPOPROTEINS IN RATS. *Lipids* 18:375-81

755 Tannock GW, Tangerman A, Vanschaik A, McConnell MA. 1994. DECONJUGATION OF BILE-ACIDS BY

756   LACTOBACILLI IN THE MOUSE SMALL-BOWEL. *Applied and Environmental Microbiology*

757   60:3419-20

758 Ulmius J, Lindblom G, Wennerstrom H, Johansson LBA, Fontell K, et al. 1982. MOLECULAR-

759   ORGANIZATION IN THE LIQUID-CRYSTALLINE PHASES OF LECITHIN SODIUM CHOLATE WATER-

760   SYSTEMS STUDIED BY NUCLEAR MAGNETIC-RESONANCE. *Biochemistry* 21:1553-60

761 Werner A, Minich DM, Havinga R, Bloks V, Van Goor H, et al. 2002. Fat malabsorption in essential fatty

762   acid-deficient mice is not due to impaired bile formation. *American Journal of Physiology-*

763   *Gastrointestinal and Liver Physiology* 283:G900-G8

764 Wiedmann TS, Kamel L. 2002. Examination of the solubilization of drugs by bile salt micelles. *Journal*

765   *of Pharmaceutical Sciences* 91:1743-64

766 Yang Y, McClements DJ. 2013. Vitamin E and Vitamin E acetate solubilization in mixed micelles:

767   Physicochemical basis of bioaccessibility. *Journal of Colloid and Interface Science* 405:312-21

768 Ziani K, Fang Y, McClements DJ. 2012. Encapsulation of functional lipophilic components in surfactant-

769   based colloidal delivery systems: Vitamin E, vitamin D, and lemon oil. *Food Chemistry*

770   134:1106-12

771

772

773 ## Graphical abstract

774

775

776

777

778

779

780

781

782

783

784

785
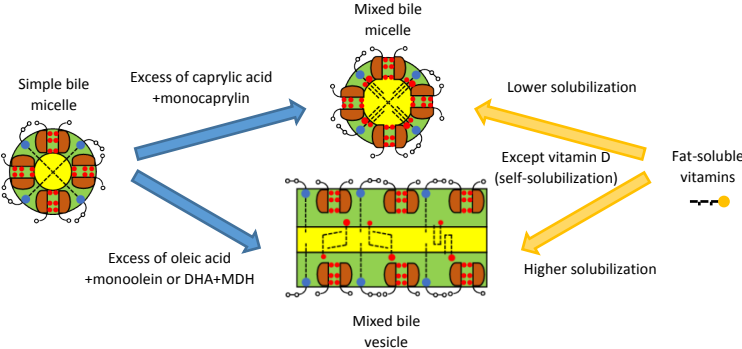
786   Asma El Aoud: Methodology, Investigation, Visualization, Formal analysis, Writing - Original Draft

787   Emmanuelle Reboul: Methodology, Supervision, Writing - Review & Editing

788   Aurélien Dupont: Investigation, Visualization

789   Cristelle Mériadec: Investigation, Visualization

790   Franck Artzner: Methodology, Investigation, Visualization, Writing - Review & Editing

791   Sébastien Marze: Conceptualization, Supervision, Project administration, Funding acquisition,
792   Methodology, Investigation, Visualization, Formal analysis, Writing - Original Draft, Writing - Review
793   & Editing

794